Mechanistic and Curtin–Hammett Studies of the $^1O_2$ Oxidation of a Prenyl Phenol and Phenolate Anion

Akshaya Iyer,[1,2] Lloyd Lapoot,[1,3] and Alexander Greer[1-3]*

[1] Department of Chemistry, Brooklyn College, City University of New York, Brooklyn, New York 11210, United States

[2] Ph.D. Program in Chemistry, The Graduate Center of the City University of New York, 365 Fifth Avenue, New York, New York 10016, United States

[3] Ph.D. Program in Biochemistry, The Graduate Center of the City University of New York, 365 Fifth Avenue, New York, New York 10016, United States

Email address: agreer@brooklyn.cuny.edu

Table of contents graphic

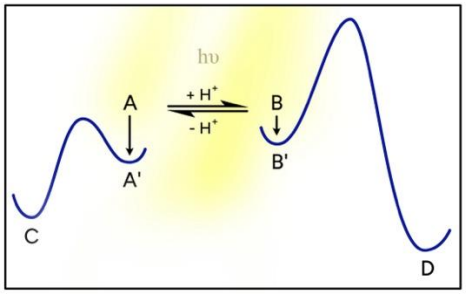

Abstract

The Curtin–Hammett principle, widely recognized in thermal reactions, has been extended to photosensitization processes in this study, providing new insights into the reactivity of photogenerated singlet oxygen ($^1O_2$) with phenol and phenolate anion species. Here, we explore mechanistic and Curtin–Hammett studies of the equilibrium between the phenol and phenolate anion forms of a prenylated natural product, prenylphloroglucinol. This study uses density functional theory (DFT) to examine phenol and phenolate anion-quenching pathways of $^1O_2$ showing distinct pathways for each form. In the phenolate anion, $^1O_2$ is quenched to form a peroxy anion. In contrast, in the phenol form, $^1O_2$ leads to a potent epoxidizing agent in a seemingly pro-oxidant path. An *iso*-hydroperoxyhydrofuran intermediate is proposed to be key in the epoxidation. Meanwhile, the phenolate anion cyclizes and protonates forming a comparatively benign hydroperoxyhydrofuran species. The phloroglucinol is next to the C-prenyated group directs the reaction pathway towards the formation of a dihydrobenzofuran, deviating from the conventional $^1O_2$ 'ene' reaction mechanism and the production of allylic hydroperoxides typically observed in trisubstituted alkenes.

1. Introduction

Concepts in physical organic chemistry, such as the Curtin–Hammett principle, Hammond's postulate, and the Thorpe-Ingold effect, are well-established for thermal reactions.[1] However, their photochemical or photosensitized counterparts have been much less explored. Notably, Bochet and Harvey described excited-state transition states (TSs) and conical

intersections (CIs) to extend to a photochemical equivalent of Hammond's postulate.[2] Building on this foundation, we investigate a photosensitized equivalent of the Curtin–Hammett principle using photogenerated singlet oxygen ($^1O_2$). More accurately, this is a photosensitized reaction to form $^1O_2$ that reacts with the phenol and the phenolate anion of prenylphloroglucinol (2-prenyl-1,3,5-benzenetriol, **1**). Excitingly (*pun intended*), we propose that they function as high-energy pro-oxidants and low-energy antioxidants, respectively, with distinct mechanistic pathways governing each reaction.

The Curtin–Hammett principle states that when two species, **A** and **B**, are in equilibrium, their product distribution is determined by the energy barriers of their reaction pathways rather than their relative populations (Figure 1). The Curtin–Hammett principle also implies that the rate of interconversion of the reacting species (**A** and **B**) should be faster than each of the distinct reactions (**A** to **C** or **B** to **D**). Here, **A** reacts to form **C** via a lower energy barrier, while **B** reacts to form **D** via a higher energy barrier. Despite the higher population of **B**, **C** dominates due to **A**'s lower transition state energy. This principle emphasizes the role of transition state energies over reactant equilibria in determining product outcomes. In analogy to the Curtin–Hammett principle, this study investigates the equilibrium between prenylphloroglucinol in its phenolate anion form (**A**) and phenol form (**B**), which gives rise to distinct species. Commonly $^1O_2$ is generated by photosensitization, which is modeled by density functional theory (DFT) in this study. This $^1O_2$ can then react with the phenolate anion (**A**) to generate an internally hydrogen-bonded perepoxide (**A'**), which subsequently leads to the formation of peroxy anion (ROO^-) (**C**). The **C** is subsequently protonated to form a dihydrobenzofuran hydroperoxide product, indicating the incorporation of $^1O_2$ into the molecule. Hence, we refer to this process as an antioxidant pathway. In contrast, the phenol (**B**) is converted into the hydrogen-bonded singlet oxygen intermediate (**B'**)

which proceeds to form an *iso*-hydroperoxy intermediate [$R(H)^{+}OO^{-}$] (**D**). As we will see, **D** undergoes epoxidation, leading to the formation of the more stable dihydrobenzofuran alcohol. Hence, we refer to this process as a pro-oxidant pathway.

Our group has been interested in photochemical processes involving $^1O_2$, and oxygen radicals and radical ions.[3,4] One facet of our work is the use of adjuvants or other compounds to amplify or deactivate oxidative reactions.[5] In this vein we focused on efforts to fine-tune $^1O_2$ oxidative processes depending on the system's needs.[6-8] This leads us to the present study on a phenol/phenolate anion system, where we propose a mechanism inspired by the Curtin–Hammett principle, but in a $^1O_2$ photosensitized context. We focused on the reaction of $^1O_2$ with a phenol and phenolate anion of prenylphloroglucinol, to try to achieve mechanistic control over product formation.

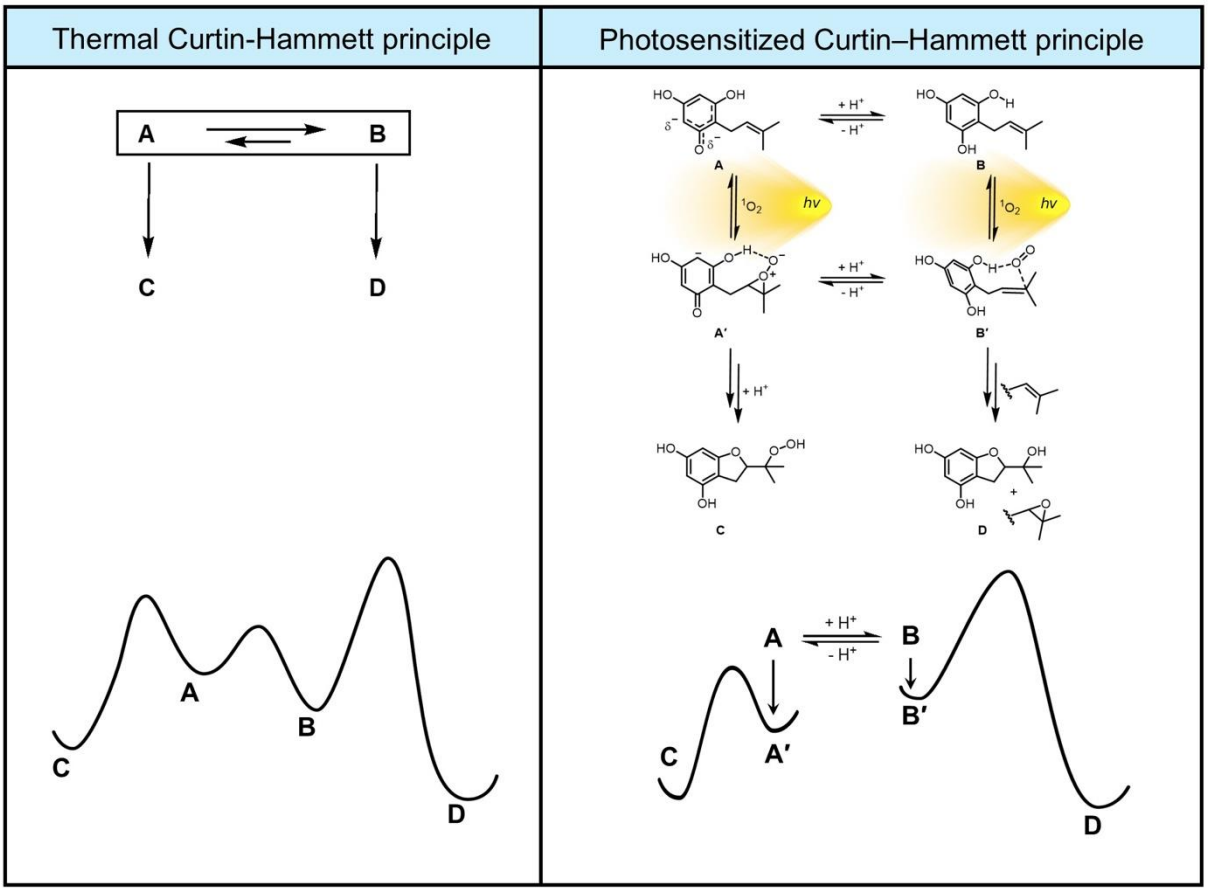

Figure 1. Illustration of thermal Curtin–Hammett (left) and $^1O_2$ photosensitized Curtin–Hammett behavior (right). Left panel: The thermal pathway shows **A** and **B** in equilibrium, where **A** forms **C** in a lower energy barrier, and **B** forms **D** in a higher energy barrier. Right panel: The $^1O_2$ photosensitized pathway depicts prenylphloroglucinol in its phenolate anion form **A** and phenol form **B** leading to the corresponding peroxy species **A'** and **B'**, where **A'** forms **C** with a lower energy barrier, and **B'** forms **D** with a higher energy barrier. In the text, labeling is as follows: **A** is **7**; **B** is **1**; **A'** is **8**; **B'** is **2**; **C** is **5**; and **D** is **4**.

2. Computational Section

M062X/6-31+G(d,p) calculations were conducted using the Gaussian16 program (revision C.01).[9] The reaction enthalpies are reported with thermal (298 K) and zero-point energy corrections.[10] Analysis of stationary points was carried out by frequency calculations. Basis set superposition error (BSSE) was computed using the counterpoise correction method of Boys and Bernardi.[10] Verification of **TS2/3**, **TS3A/4**, **TS 3/5**, **TS3/6**, and **TS8/9** were also carried out by tracing their internal reaction coordinates (IRC); the forward directions of **TS9/10** and **TS9'** were also verified. Single point calculations were also conducted. In our previous reports on DFT calculations of the $^1O_2$ oxidation of glycocitrine and prenyl surfactant,[11,12] T1 diagnostics were found to not problematic with spin contamination having reasonable T1 values. To account for water solvent effects, we also carried out conductor-like polarized continuum model (CPCM) calculations.[13] The proton affinities (PA) of various phenolate anions and peroxy anions were calculated to reveal insights into their acid-base behavior. The singlet–triplet gap of $^1O_2$ ($^1\Delta_g$) is known to be 22.5 kcal/mol experimentally, thus we calculated $^1O_2$ ($^3\Sigma_g^+$) and added the 22.5 kcal/mol energy to it.

3. Results and Discussion

Described next are the results of our DFT study, including the energetics of phenol and phenolate anion, reaction prenylated phloroglucinol **1** with $^1O_2$ oxidation, and computed routes for the phenol path A-D and phenolate anion path E-I.

3.1 Proton Affinities of the Phenolate Anion and a Related Peroxy Anion. In Figure 2, the DFT calculated PA of phenolate anion **7** (341.7 kcal/mol) is found to be more exothermic than

its corresponding anion formed after reaction with $^1O_2$ **8** (313.7 kcal/mol). Here, **2** should not be considered the "protonated" form of **8**, but rather a protonated form followed by endothermic rearrangements. Interestingly, anion **7** bears greater nucleophilicity relative to **1**, and single-point calculations indicate that the phenolate anion **7** is higher in energy than phenol **1**, and that the perepoxide **8** is lower in energy than the H-bonded $^1O_2$-phenol complex **2**. We believe that the Curtin–Hammett principle can be applied to this reaction since phenol **1** and phenolate anion **7** are rapidly equilibrating species. Next, sections 3.2 and 3.3, show the mechanistic divergence between the neutral **2** and anionic **8** pathways result in different outcomes, namely one being pro-oxidant and the other being antioxidant in character.

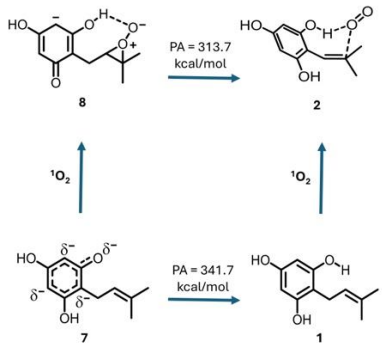

Figure 2. Calculated proton affinities (PA). Gas-phase data are in kcal/mol for M062X/6-31+G(d,p).

3.2 Phenol Path: $^1O_2$ Oxidation of the Prenyl Site. In Figure 3, **1** was seen to have an internal O–H···π bond with the prenyl C=C group. With the approach of $^1O_2$ to the prenyl group, a perepoxide intermediate was not found, where instead $^1O_2$ forms an intermolecular H-bond with

an adjacent OH group to reach **2**. In the absence of such intermolecular H-bonds, simple alkenes can react with $^1O_2$ through a perepoxide transition state and subsequent bifurcation on the potential energy surface (PES) to allylic hydroperoxides.[12,14-16] Path A shows the interconversion of **2** to *iso*-hydroperoxide **3** via **TS2/3**. Based on subsequent low 10.3 kcal/mol barrier (**TS3A/4**), *iso*-hydroperoxide **3** is judged to be a powerful oxidant with a facile O-atom transfer to the prenyl group of a neighboring **1** molecule. The epoxidation reaction to reach **4** is computed to be relative to **3** and 2-methyl-2-butene, where 2-methyl-2-butene is a model for the prenyl group of another molecule of **1**. The epoxidation of the C=C bond of 2-methyl-2-butene (as a model for **1**) by **3** produces an alcohol byproduct, **4**, and is exothermic by 87.9 kcal/mol (path B). For **TS3A/4**, BSSE corrected complexation energy was found to be –22.7 kcal/mol, which differed by only 0.82 kcal/mol when compared to the uncorrected (raw) complexation energy of –23.5 kcal/mol. The conversion of *iso*-hydroperoxide **3** to hydroperoxide **5** proceeds by a slightly higher energy **TS3/5** in a process that is exothermic by only 36.8 kcal/mol. Similarly, dihydrobenzofuran **6** can form through H_2O_2 expulsion from **3** by **TS3/6** in an even less exothermic reaction of 21.8 kcal/mol.

Calculations were also explored in aqueous solution as modeled with CPCM, and were found to have fairly minor effects on the energetics. For example, the energy barrier for the conversion of **2** to *iso*-hydroperoxide **3** via **TS2/3** was reduced by 5.9 kcal/mol compared to the gas phase, indicating a stabilization effect due to solvation and intermolecular interactions. The epoxidation reaction from **3** and 2-methyl-2-butene led to **TS3A/4** with a producing **4** was reduced by 3.2 kcal/mol compared to the gas phase and slightly more exothermic. By contrast, the TSs leading from **3** to **5** or **6** were slightly higher compared to the gas phase. The formation of hydroperoxide **5** and dihydrobenzofuran **6** were less exothermic by ~3 kcal/mol compared to the gas phase.

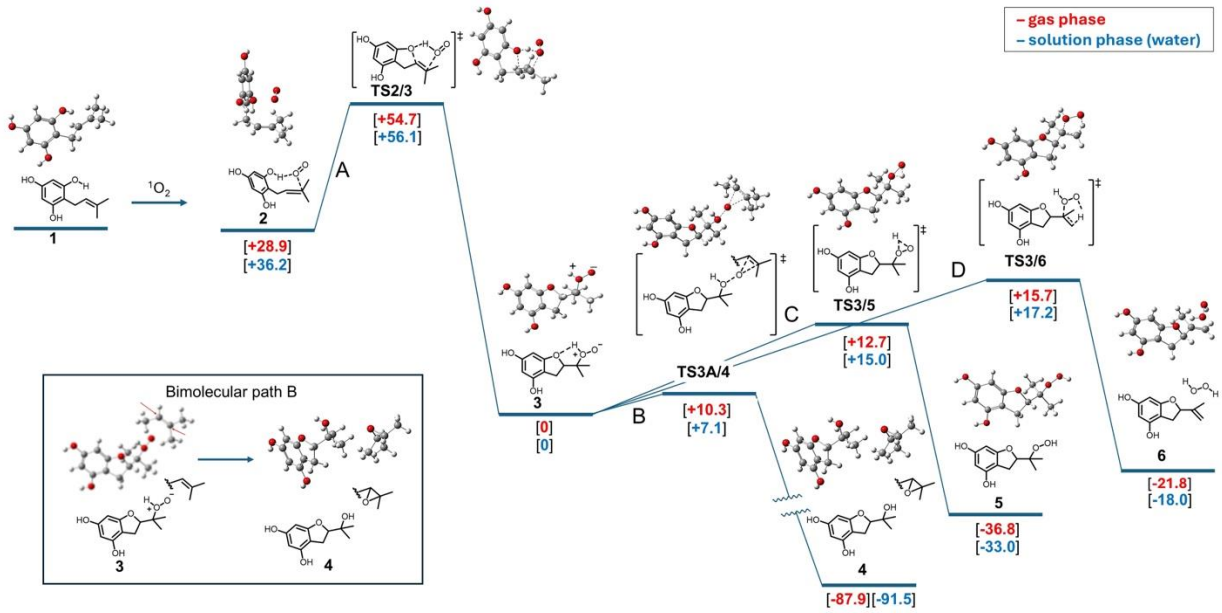

Figure 3. Calculated potential energy surface for the reaction of phenol **1** with $^1O_2$. Gas-phase and solution-phase energetics are in kcal/mol for M062X/6-31+G(d,p). Energies of **2**, **5**, and **6**, are relative to 2-(2-*iso*-hydroperoxypropan-2-yl)-2,3-dihydrobenzofuran-4,6-diol **3**. The energy of **4** is relative to **3** and 2-methyl-2-butene. Inset: epoxidation of C=C bond of 2-methyl-2-butene by **3**.

3.3 Phenolate Anion Path: $^1O_2$ Oxidation of the Prenyl Site. In Figure 4, **7** was found to form an unsymmetrical perepoxide **8**, in which the incoming $^1O_2$ forms a H-bond with an adjacent OH group. Notice that perepoxide **8** resides in a fairly shallow minimum, in which its formation may involve a valley-ridge inflection (VRI) eventually leading to **9** (we will discuss on this point below). Path E shows the interconversion of **8** to peroxy anion **9** via **TS8/9** with an energy of 3.3 kcal/mol. An 11.7 kcal/mol barrier in **TS9'** is computed which involves subsequent steps to reach carbanion **11** (paths F and G) in an endothermic process. Indeed, carbanion **11** is

computed to be slightly higher in energy than **TS9'**. An even higher and more endothermic path than F is H in the conversion of **9** to **10** via **TS9/10**. Path I shows the path that we think is most likely, a facile protonation of **9** to reach **5** (see box in Figure 4). The calculated PA of anion **7** relative to prenylphloroglucinol **1** is 341.7 kcal/mol. This value is similar to literature reports of PA of the parent phenolate anion relative to phenol calculated using M06-2X/6-311++G(d,p) which was 347.2 kcal/mol.[17] For anion **9**, the PA relative to hydroperoxide **5** is calculated as 363.5 kcal/mol, indicating that protonation at the outer oxygen is more favorable. This suggests that protonation at the internal oxygen of the O–O group in **ISO 3**, with a PA of 326.5 kcal/mol, is less favorable due to the lower basicity of the internal oxygen. Our computed values are understandable when compared to experimental PA reports of hydroxide anion (393.8 kcal/mol) and methoxide anion (381.7 kcal/mol) are higher relative to acetate anion (348.1 kcal/mol).[18] We note that unlike Figure 3 for the neutral path, in the anionic path in Figure 4, an epoxidation was not found for a reaction with **9** and 2-methyl-2-butene, where the peroxy anion of **9** appears to have repulsion for the C=C bond of 2-methyl-2-butene. The conversion of peroxy anion **9** to dihydrobenzofuran is computed to take place through HOO^- via **TS9/10** in an endothermic reaction of 13.9 kcal/mol.

Calculations in aqueous solution, modeled using CPCM, revealed moderate deviations in energetics compared to the gas phase, pointing to the influence of solvation. For instance, the energy barrier for the conversion of **8** to peroxy anion **9** via **TS8/9** increased by 2.6 kcal/mol. The conversion of **9** through **TS9'** to eventually reach **11** in path F showed a more pronounced increase of 9.7 kcal/mol in the energy barrier for a more endothermic process in solution. Similarly, the conversion of **9** to **10** through **TS9/10** in path H exhibited an increase of 6 kcal/mol in the energy barrier, again becoming more endothermic.

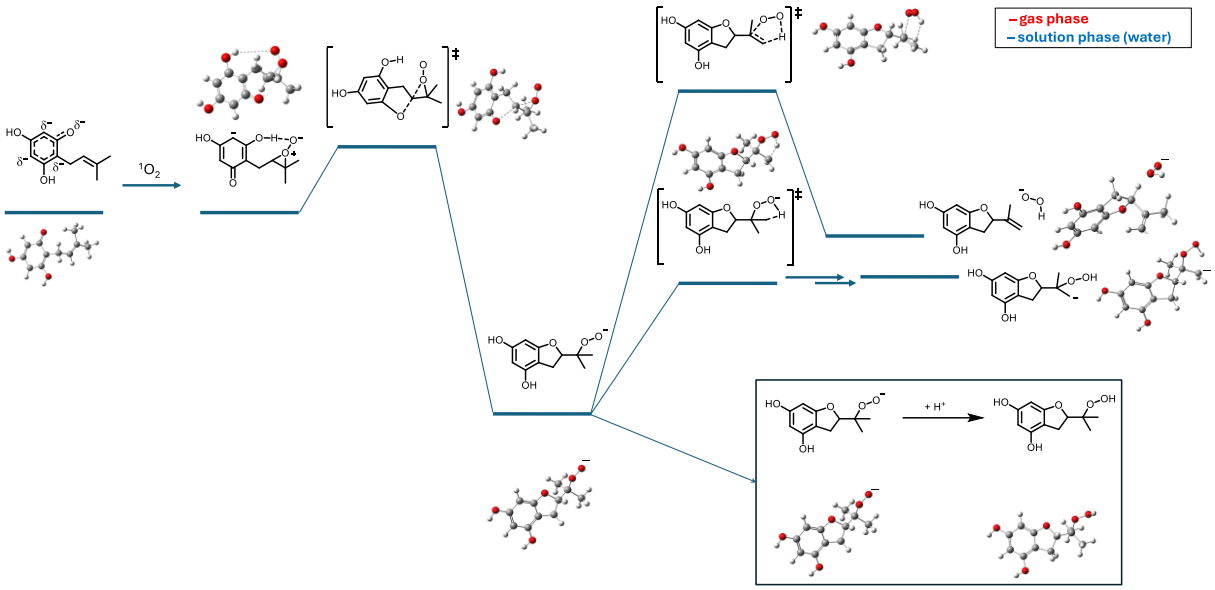

Figure 4. Calculated potential energy surface for the reaction of phenolate anion **1** with $^1O_2$. Gas-phase and solution-phase energetics are in kcal/mol for M062X/6-31+G(d,p). Energies of **8**, **10**, and **11**, are relative to 2-(2-peroxypropan-2-yl)-2,3-dihydrobenzofuran-4,6-diol anion **9**. Inset: proton affinity of **9**.

4. Mechanism

We build upon the Curtin–Hammett principle and an extension to the phenol/phenolate equilibrium of prenylphloroglucinol **1** and their reactions with $^1O_2$. These reactions with the phenol **2** and phenolate anion **7** are facile with first-excited state of $^1O_2$ ($^1\Delta_g$), which is elevated by 22.5 kcal/mol relative to ground-state triplet oxygen.

Our DFT results are comparable with the experimentally observed reactivity of $^1O_2$ with phenols and phenolate anions, in which our calculations show a lower energy pathway for the reaction of $^1O_2$ with the phenolate anion **7** compared to the phenol **1**. Experimental data,

summarized in Table 1, indicate that the total quenching rate constants (k_T) and chemical quenching rate constants (k_r) for $^1O_2$ reactions with phenolate anions are higher than those for phenols, with $k_{phenolate}/k_{phenol}$ ratios ranging from ~16 to ~16,000. As anticipated, the more nucleophilic phenolate anion reacts more readily with electrophilic $^1O_2$. However, the comparison of the experimental data in Table 1 with our DFT results is limited due to the structural differences between the systems. Our model features a prenyl group and a polyphenol with three alcohol groups, whereas the compounds in Table 1 are for simpler phenols and phenolate anions.

Expanding on the mechanistic behavior of phenol and phenolate anion forms of prenylphloroglucinol in their reactions with $^1O_2$, this study highlights a unique aspect of $^1O_2$ chemistry, specifically epoxidation. While $^1O_2$ reactions are most commonly associated with 'ene' reactions, as well as [2 + 2] and [2 + 4] cycloadditions yielding allylic hydroperoxides,[4,19-21] dioxetanes and endoperoxides,[22-24] respectively, epoxidation is less commonly observed.[25-28] In our case, the phenol form of prenyphloroglucinol, as opposed to its phenolate anion form, shows a predicted epoxidation pathway by oxygen transfer from the *iso*-hydroperoxide intermediate. This is a proposed bimolecular reaction with an alkene moiety of the reagent. The mechanistic divergence between the phenol **2** and phenolate anion **7** in this study provides a unique platform to investigate this underexplored aspect of $^1O_2$-mediated oxidative pathways. The phenolate anion **7** forms perepoxide **8** within a shallow minimum, indicating its transient nature as an intermediate. In this context, the phenolate anion leads to a perepoxide **8** that is close to its transitional state **TS8/9**, where solvation stabilizes it by 2.6 kcal/mol, making **8** a more full-fledged intermediate. The shallow minimum for the perepoxide **8** in Figure 4 is more prevalent in the gas phase with reduced "intermediate" character. This type of PES tuning evokes similarities to asynchronous bond formation processes characterized by VRI.[12,14-16,29,30] Notably, recent studies have identified

a distinct solvation pattern, highlighting a perepoxide transition state in a gas-phase environment.[12] This continuum extends to the other end of the spectrum, leading to a perepoxide intermediate under protic environment, illustrating the influence of environmental factors on the reaction pathway.

The chemistry of enol/enolate anions in $^1O_2$ mediated processes remains sparsely studied and is in need of further exploration.[31-33] The reactivity of prenylphloroglucinol **1** with $^1O_2$ shows some similarities to natural compounds like hyperforin (Figure 5),[34] but also exhibits differences. Prior DFT studies on hyperforin revealed that its enol/enolate anion core, surrounded by four prenyl groups, is reactive to $^1O_2$, in particular the southwest and southeast quadrants relative to the northwest and northeast quadrants forming hydroperoxides through the $^1O_2$ 'ene' reaction. Our current DFT studies of prenylphloroglucinol **1** shares a similarity to hyperforin in that it reacts with $^1O_2$. However, it diverges mechanistically, proceeding through *iso*-hydroperoxide and peroxy anion intermediates. These pathways result in the formation of epoxide, alcohol, and non-'ene' hydroperoxide products, highlighting a distinct reactivity profile.

Table 1. Literature data on total quenching rate constants (k_T) and chemical quenching rate constants (k_r) of the reaction of $^1O_2$ with substituted phenols and phenolate anions

entry	phenols	k_T (M^{-1} s^{-1})[a] or k_r (M^{-1} s^{-1})[b]	phenolate anions	k_T (M^{-1} s^{-1})[b] or k_r (M^{-1} s^{-1})[c]	ratio of $k_{phenolate}/k_{phenol}$
1	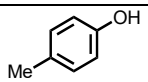	1.0×10^{7}[c]	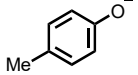	3.5×10^{8}[c] 6.7×10^{8}[c]	~35-67
2	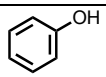	$<10^{4}$		7.0×10^{7}[b] 1.6×10^{8}[c]	~7000-16000
3	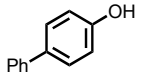	7.3×10^{4}[b]	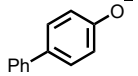	1.0×10^{7}[c]	~137
4	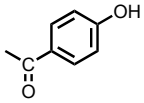	1.5×10^{6}[c]	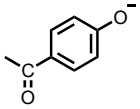	2.4×10^{7}[b]	~16
5	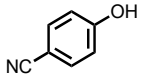	2.0×10^{5}[c]	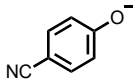	6.2×10^{6}[c]	~31
6	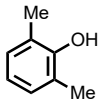	3.6×10^{7}[c]	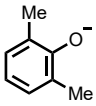	8.6×10^{8}[c]	~24

Data acquired from ref 35.

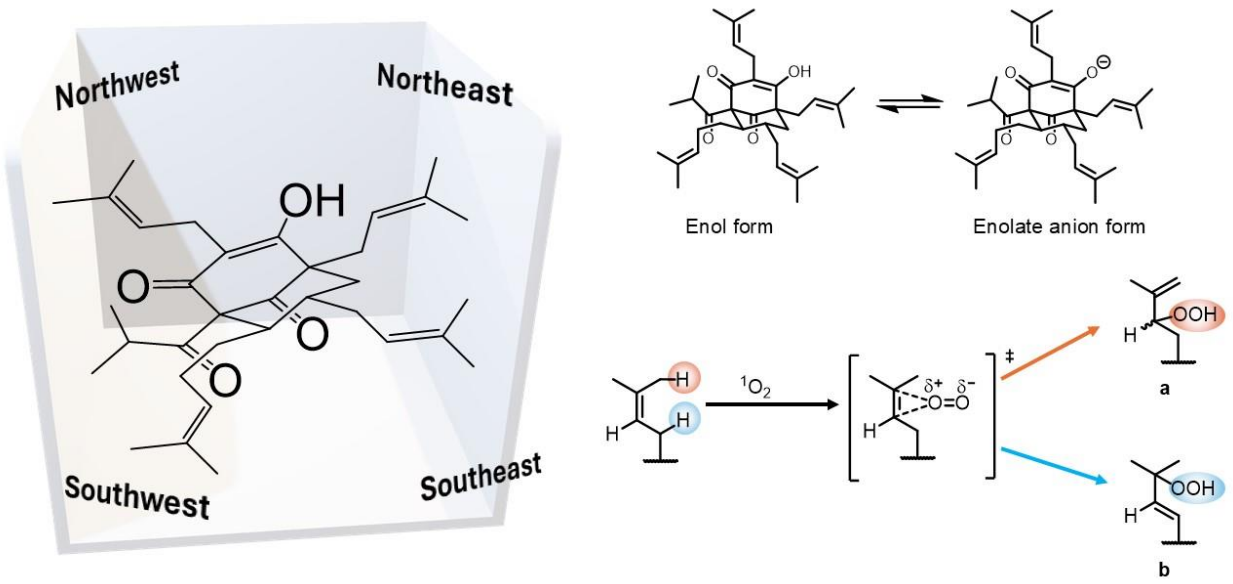

Figure 5. Hyperforin quadrants, enol/enolate forms, and the $^1O_2$ 'ene' reaction.

5. Summary

In this study, we propose Curtin–Hammett behavior to explain the reactivity of $^1O_2$ with prenylphloroglucinol **1**, based on the energetics obtained through DFT. Typical Curtin–Hammett behavior is when two species are in equilibrium, their product distribution is determined by the energy barriers of their respective reaction pathways, rather than their relative concentrations. In our system, the base/acid equilibrium between the phenolate anion form **7** and the phenol form **1** of prenylphloroglucinol lead to distinct reaction pathways upon exposure to $^1O_2$. Rather than the relative energy differences between **1** and **7**, the activation energies of their transition states are key to understanding the outcome of the reaction.

The phenolate anion **7** reacts with $^1O_2$ to form a perepoxide intermediate **8**. The transition state **TS8/9** for this reaction has an energy barrier of 3.3 kcal/mol, leading to the formation of the peroxy anion (ROO^-) intermediate **9**. This intermediate undergoes a protonation step, resulting in

the formation of a non-'ene' hydroperoxide product **5** (Figure 4, inset). This pathway is similar to the Curtin–Hammett principle, where **8** proceeds through a lower-energy transition state **TS8/9**, compared to **2** with its higher-energy transition state **TS2/3**. The former leads to peroxy anion **9** and then **10**, and the latter leads to an *iso*-hydroperoxide intermediate **3**, which undergoes an O-transfer step, resulting in the formation of an epoxide and dihydrobenzofuran alcohol **4**.

Pro-oxidant and Antioxidant Pathways? Our DFT results implicate pro-oxidant (epoxidation) and antioxidant (non-'ene' hydroperoxidation) processes in the $^1O_2$ oxidation phenol and phenolate anion of prenylphloroglucinol. As we mentioned above, our results point to an interconversion between prenylphloroglucinol *iso*-hydroperoxy [$R(H)^+OO^-$] and peroxy anion (ROO^-) intermediates to reach dihydrobenzofuran alcohol or dihydrobenzofuran hydroperoxide products. A key determinant is that the phenol form leads to an *iso*-hydroperoxide leads to facile epoxidation, which attribute to a pro-oxidant path. On the other hand, the phenolate anion form leads to a comparatively stable non-'ene' hydroperoxide product that incorporated $^1O_2$ and thus referred to as an antioxidant path.

6. Conclusion

The above system demonstrates similarities to the Curtin–Hammett principle. The higher activation energy of the reaction pathway through **TS2/3** allows for the formation of an *iso*-hydroperoxide intermediate, but leads to the energetically favorable epoxide product. In the future, experimental studies can address prenylphloroglucinol photooxidations under Brønsted acidic and basic conditions to assess whether both pro-oxidant and antioxidant pathways occur. One challenge will be finding a photosensitizer system with identical $^1O_2$ quantum yields under varying acid and base conditions.

ORCID

Akshaya Iyer: 0000-0001-5499-2672

Lloyd Lapoot: 0000-0001-6888-2626

Alexander Greer: 0000-0003-4444-9099

Supporting Information

Supporting Information is available, which includes: Energies and Cartesian Coordinates of structures computed with M062X/6-31+G(d,p).

Acknowledgments

We thank the National Science Foundation (CHE-2154133) for funding. We also thank Leda Lee for assistance with the graphic arts work.

References

1. Carey, F. A.; Sundberg, R. J. *Advanced Organic Chemistry, Part A: Structure and Mechanisms*, 5th ed.; Plenum Press: New York, 2007, pp 289-293, 296-297.
2. Bochet, C. G.; Harvey, F. M. Is there a Photochemical Hammond Postulate? *Chem. Sci.* **2021**, *12*, 599–605.
3. Baptista, M. S.; Cadet, J.; Greer, A.; Thomas, A. H. Practical Aspects in the Study of Biological Photosensitization Including Reaction Mechanisms and Product Analyses: A Do's and Don'ts Guide. *Photochem. Photobiol.* **2023**, *99,* 313-334.

4. Ghogare, A. A.; Greer, A. Using Singlet Oxygen to Synthesize Natural Products and Drugs. *Chem. Rev.* **2016**, *116*, 9994–10034.
5. Lapoot, L.; Jabeen, S.; O'Connor, R. M.; Korytowski, W.; Girotti, A.; Greer, A. Photosensitized Oxidative Damage from a New Perspective: The Influence of Before-Light and After-light Reaction Conditions. *J. Org. Chem.* **2024**, *89*, 12873–12885.
6. Jabeen, S.; Farag, M.; Malek, B.; Choudhury, R.; Greer, A. Singlet Oxygen Priming Mechanism: Disentangling of Photooxidative and Downstream Dark Effects. *J. Org. Chem.* **2020**, *85*, 12505–12513.
7. Jabeen, S.; Ghosh, G.; Lapoot, L.; Durantini, A. M.; Greer, A. Sensitized Photooxidation of ortho-Prenyl Phenol: Biomimetic Dihydrobenzofuran Synthesis and Total $^1O_2$ Quenching. *Photochem. Photobiol.* **2023**, *99*, 637–641.
8. Durantini, A. M.; Lapoot, L.; Jabeen, S.; Ghosh, G.; Bipu, J.; Essang, S.; Singh, B. C.; Greer, A. Tuning the $^1O_2$ Oxidation of a Phenol at the Air/Solid Interface of a Nanoparticle: Hydrophobic Surface Increases Oxophilicity. *Langmuir* **2023**, *39*, 11134–11144.
9. Frisch, M. J.; Trucks, G. W.; Schlegel, H. B.; Scuseria, G. E.; Robb, M. A.; Cheeseman, J. R.; Scalmani, G.; Barone, V.; Petersson, G. A.; Nakatsuji, H.; Li, X.; Caricato, M.; Marenich, A. V.; Bloino, J.; Janesko, B. G.; Gomperts, R.; Mennucci, B.; Hratchian, H. P.; Ortiz, J. V.; Izmaylov, A. F.; Sonnenberg, J. L.; Williams-Young, D.; Ding, F.; Lipparini, F.; Egidi, F.; Goings, J.; Peng, B.; Petrone, A.; Henderson, T.; Ranasinghe, D.; Zakrzewski, V. G.; Gao, J.; Rega, N.; Zheng, G.; Liang, W.; Hada, M.; Ehara, M.; Toyota, K.; Fukuda, R.; Hasegawa, J.; Ishida, M.; Nakajima, T.; Honda, Y.; Kitao, O.; Nakai, H.; Vreven, T.; Throssell, K.; Montgomery, J. A. Jr.; Peralta, J. E.; Ogliaro, F.;

Bearpark, M. J.; Heyd, J. J.; Brothers, E. N.; Kudin, K. N.; Staroverov, V. N.; Keith, T. A.; Kobayashi, R.; Normand, J.; Raghavachari, K.; Rendell, A. P.; Burant, J. C.; Iyengar, S. S.; Tomasi, J.; Cossi, M.; Millam, J. M.; Klene, M.; Adamo, C.; Cammi, R.; Ochterski, J. W.; Martin, R. L.; Morokuma, K.; Farkas, O.; Foresman, J. B.; Fox, D. J. *Gaussian 16 Revision C.01*; Gaussian, Inc.: Wallingford, CT, 2016.

10. Jensen, F. *Introduction to Computational Chemistry*; John Wiley & Sons Inc: New Jersey, 2017.
11. Lapoot, L.; Jabeen, S.; Durantini, A. M.; Greer, A. Role of Curvature in Acridone for $^1O_2$ Oxidation of a Natural Product Homoallylic Alcohol: A Novel *Iso*-hydroperoxide Intermediate. *Photochem. Photobiol.* **2024**, *100*, 455–464.
12. Malek, B.; Lu, W.; Mohapatra, P. P.; Walalawela, N.; Jabeen, S.; Liu, J.; Greer, A. Probing the Transition State-to-Intermediate Continuum: Mechanistic Distinction Between a Dry vs Wet Perepoxide in the Singlet Oxygen 'Ene' Reaction at the Air-Water Interface. *Langmuir* **2022**, *38*, 6036–6048.
13. Cossi, M.; Rega, N.; Scalmani, G.; Barone, V. Energies, Structures, and Electronic Properties of Molecules in Solution with the C-PCM Solvation Model. *J. Comput. Chem.* **2003**, *24*, 669–681.
14. Leach, A. G.; Houk, K. N.; Foote, C. S. Theoretical Prediction of a Perepoxide Intermediate for the Reaction of Singlet Oxygen with *trans*-Cyclooctene Contrasts with the Two-Step No-Intermediate Ene Reaction for Acyclic Alkenes. *J. Org. Chem*. **2008**, *73*, 8511–8519.

15. Singleton, D. A.; Szymanski, M. J.; Meyer, M. P.; Leach, A. G.; Kuwata, K. T.; Chen, J. S.; Greer, A.; Foote, C. S.; Houk, K. N. Mechanism of Ene Reactions of Singlet Oxygen: A Two-Step No-Intermediate Mechanism. *J. Am. Chem. Soc.* **2003**, *125*, 1319–1328.
16. Griesbeck, A. G.; Goldfuss, B.; Jäger, C.; Brüllingen, E.; Lippold, T.; Kleczka, M. Strong Asymmetry in the Perepoxide Bifurcation Mechanism: The Large-Group Effect in the Singlet Oxygen Ene Reaction with Allylic Alcohols. *ChemPhotoChem* **2017**, *1*, 213–221.
17. Cagardová, D.; Michalík, M.; Klein, E.; Lukeš, V.; Marković, Z. DFT and Calculations of Ionization Potentials, Proton Affinities, and Bond Dissociation Enthalpies of Aromatic Compounds. *Acta Chim. Slovaca* **2019**, *12*, 225–240.
18. NIST Computational Chemistry Comparison and Benchmark Database, NIST Standard Reference Database Number 101, Release 22; Johnson, R. D., III, Ed.; May 2022. Available at: http://cccbdb.nist.gov/.
19. Alberti, M. N.; Orfanopoulos, M. Unraveling the Mechanism of the Singlet Oxygen Ene Reaction: Recent Computational and Experimental Approaches. *Chem. Eur. J.* **2010**, *16*, 9414–9421.
20. Alberti, M. N.; Orfanopoulos, M. Recent Mechanistic Insights in the Singlet Oxygen Ene Reaction. *Synlett* **2010**, *7*, 999–1026.
21. Manring, L. E.; Kanner, R. C.; Foote, C. S. Chemistry of Singlet Oxygen. 43. Quenching by Conjugated Olefins. *J. Am. Chem. Soc.* **1983**, *105*, 4707–4710.
22. Balci, M. Bicyclic Endoperoxides and Synthetic Applications. *Chem. Rev.* **1981**, *81*, 91–108.
23. Clennan, E. L. Synthetic and Mechanistic Aspects of 1,3-Diene Photooxidation. *Tetrahedron* **1991**, *47*, 1343–1382.

24. Clennan, E. L.; Foote, C. S. In *Organic Peroxides*; Ando, W., Ed.; Wiley: Chichester, UK, **1992**; 255–318.

25. Akasaka, T.; Sakurai, A.; Ando, W. Cooxidation Reaction in the Singlet Oxygenation of Cyclic and Benzylic Sulfides: *S*-Hydroperoxysulfonium Ylide Intermediate as a New Epoxidizing Species. *J. Am. Chem. Soc.* **1991**, *113*, 2696-2701.

26. Sauter, M.; Adam, W. Oxyfunctionalization of Benzofurans by Singlet Oxygen, Dioxiranes, and Peracids: Chemical Model studies for the DNA-Damaging Activity of Benzofuran Dioxetanes (Oxidation) and Epoxides (Alkylation). *Acc. Chem. Res.* **1995**, *28*, 289–298.

27. Poon, T. H. W.; Pringle, K.; Foote, C. S. The Reaction of Cyclooctenes with Singlet Oxygen. Trapping of a Perepoxide Intermediate. *J. Am. Chem. Soc.* **1995**, *117*, 7611–7618.

28. Greer, A.; Chen, M.-F.; Jensen, F.; Clennan, E. L. Experimental and Ab Initio Computational Evidence for New Peroxidic Intermediates (Iminopersulfinic Acids). Substituent Effects in the Photooxidations of Sulfenic Acid Derivatives. *J. Am. Chem. Soc.* **1997**, *119*, 4380–4387.

29. Chuang, H. H.; Tantillo, D. J.; Hsu, C. P. Construction of Two-Dimensional Potential Energy Surfaces of Reactions with Post-Transition-State Bifurcations. *J. Chem. Theory Comput.* **2020**, *16*, 4050–4060.

30. Hare, S. R.; Tantillo, D. J. Post-Transition State Bifurcations Gain Momentum–Current State of the Field. *Pure Appl. Chem.* **2017**, *89*, 679–698.

31. Yoshioka, M.; Sakuma, Y.; Saito, M. The Effect of Solvent Polarity on the Product Distribution in the Reaction of Singlet Oxygen with Enolic Tautomers of 1-(2′,4′,6′-Trialkylphenyl)-2-Methyl 1,3-Diketones. *J. Org. Chem.* **1999**, *64*, 9247–9250.
32. Frimer, A. A.; Ripstos, S.; Marks, V.; Aljadeff, G.; Hameiri-Buch, J.; Gilinsky-Sharon, P. The Photosensitized Oxidation of α-Keto Enols: A Singlet Oxygen Approach to 2-Oxasteroids. *Tetrahedron* **1991**, *47*, 8361–8372.
33. Young, R. H.; Hart, H. The Photooxidation of an Enolate Anion: Evidence for Singlet Oxygen as the Intermediate. *Chem. Commun.* **1967**, *16*, 827–828.
34. Abramova, I.; Rudshteyn, B.; Liebman, J.; Greer, A. Computed Regioselectivity and Conjectured Biological Activity of Ene Reactions of Singlet Oxygen with the Prenylnatural Product Hyperforin. *Photochem. Photobiol.* **2017**, *93*, 626–631.
35. Wilkinson, F.; Helman, W. P.; Ross, A. B. Rate Constants for the Decay and Reactions of the Lowest Electronically Excited Singlet State of Molecular Oxygen in Solution. An Expanded and Revised Compilation. *J. Phys. Chem. Ref. Data* **1995**, *24*, 663–677.